Progressive Damage Failure Analysis of a Multi-Stringer Post-Buckled Panel

Jason Action[1]
Lockheed Martin, Marietta, Georgia, 30060

Frank A. Leone [2]
NASA Langley Research Center, Hampton, Virginia, 23681

Validation of a progressive damage finite element analysis model using the CompDam material model was performed on a large multi-stringer panel subjected to compressive loading. The panel had a Teflon insert embedded between the skin panel and stiffener to cause an ultimate failure mode of stiffener separation. The compressive loading of the panel caused the skin between the stiffeners to locally buckle before any damage began to occur. The post-buckled behavior of the panel was the driving mechanism to the onset of damage and the damage growth that led to skin-stiffener separation. An integrated global-local modeling approach was used to validate several aspects the overall behavior of the panel from start to failure. The global region captured the pre-buckled stiffness of the test panel within 10% and the buckling load of the skin panel at the critical location within 2%. The skin's five half-wave buckled mode shape was accurately predicted by the model. The integrated local model captured the load corresponding to the onset of damage within 5% of the average test data. Comparisons are made for key aspects of the damage morphology, such as a growth pattern that included a significant matrix split in the first ply of the skin and a migration of the delamination from the skin-stiffener interface to the skin's ply1-ply2 interface. The ultimate failure mode was shown to be an unstable growth of delamination damage under the stiffeners which led to a peak load of the analysis that was approximately 5% above the average peak load of the testing. The validated global-local modeling approach used on the multi-stringer post-buckled panel with a Teflon insert used a methodology and lessons learned using smaller specimens applied to a subcomponent that captured several aspects of a modern aircraft design.

Nomenclature

ACP	=	Advanced Composites Project
PDFA	=	Progressive Damage and Failure Analysis
V&V	=	Verification and Validation
G_C	=	Crack Initiation Fracture Toughness
G_R	=	Fully Developed Resistance Curve Fracture Toughness

I. Introduction

Advancements in computer technology have enabled analysts and designers of aircraft structure to incorporate difficult details and include damage progression methodologies into their analysis processes. Implementing a verified and validated method is key to obtaining an accurate solution for the structure being analyzed. The objective of the Progressive Damage and Failure Analysis (PDFA) team of NASA's Advanced Composite Project (ACP) is to develop improved PDFA methods that can reliably predict the onset and growth of damage in composite structures, leading to

[1] Aeronautical Engineer Staff, Advanced Development Programs, Associate Member
[2] Research Aerospace Engineer, Durability, Damage Tolerance, and Reliability Branch

their ultimate failure under both static and fatigue loading. Reliable methods can save time in the design and certification process by allowing key design drivers to be assessed earlier in the design process, enabling a potential reduction in physical testing required while at the same time reducing the probability of later certification tests uncovering issues that would require costly redesigns.

The methods that the PDFA team focused on during the ACP were subjected to a robust verification and validation (V&V) effort to address fundamental intralaminar, interlaminar, and interacting interlaminar/intralaminar damage modes of composite structures. A part of the validation effort of the methods involves a skin and stringer subcomponent that is representative in geometry and loading of an aircraft's wing or fuselage skin. The PDFA team chose the CompDam material model [1] for validation with the skin-stringer subcomponent. CompDam is a continuum damage mechanics methodology for fiber-reinforced composite materials that is implemented as a VUMAT user material subroutine compatible with Abaqus/Explicit analyses.

This paper shows the validation of the CompDam PDFA method for an aircraft subcomponent-sized panel that is significantly larger than other sub-element and coupon-sized configurations previously explored [2]. The validation steps include detailed comparisons to test data for a compressively loaded skin-stringer panel. The validation considers events such as pre-buckled stiffness, buckling load, mode shapes, post-buckling behavior, crack initiation and propagation, migrations of the crack to other ply interfaces and peak load. The results of the validation effort show the method's ability to capture key pre-peak failure events that contribute to the ultimate failure mode of the panel.

II. Panel Configuration

The subcomponent chosen for analysis validation was a co-cured four-stringer test panel that was 29.5 inches long by 30.3 inches wide, shown in Figure 1 [3]. The design of this panel included hat-shaped stiffeners that spanned the full length of the panel. Each stiffener was built with inner and outer wrap fabric plies to form a continuous interface between the stiffener and the skin. The skin was a 12-ply tape layup with a 24-ply padup area on the upper and lower 3.3 inches of the panel. The ramp from the 12-ply skin layup to the 24-ply padup was 1.8 inches long and followed a 20:1 ply drop off rate. The assembled test panel was designed to generate a loading condition in which a crack might grow in the skin-stiffener interface. This was achieved by first buckling the skin between the stiffeners with compression loading of the panel. Additional compressive loading beyond the initial skin buckling load amplified the post-buckled shape of the skin which generated a pull-off loading condition between the stiffener and the skin at some locations along the length of the stiffeners. The locations of the four stringers were chosen to focus the damage area to be in the center of the panel. The first and fourth stiffeners were located near the free edges of the panel. This provided stability to the free edges of the skin and prevented a crippling failure mode throughout the duration of the test. The second and third stringers of the panel were positioned to create three local skin bays that buckled due to the compressive loading. The center skin bay had a width of 4.26 inches while the outer skin bays had a slightly smaller width of 4.06 inches. All three skin bays had a length of 19.4 inches between the ramps to the padup areas. This design caused the center skin bay to buckle before the outer skin bays during the test. To further promote a delamination-dominated failure mode for analysis validation, a 0.25-inch Teflon strip was included between the hat flange and the skin of the two center stiffeners, as shown in Figure 2.

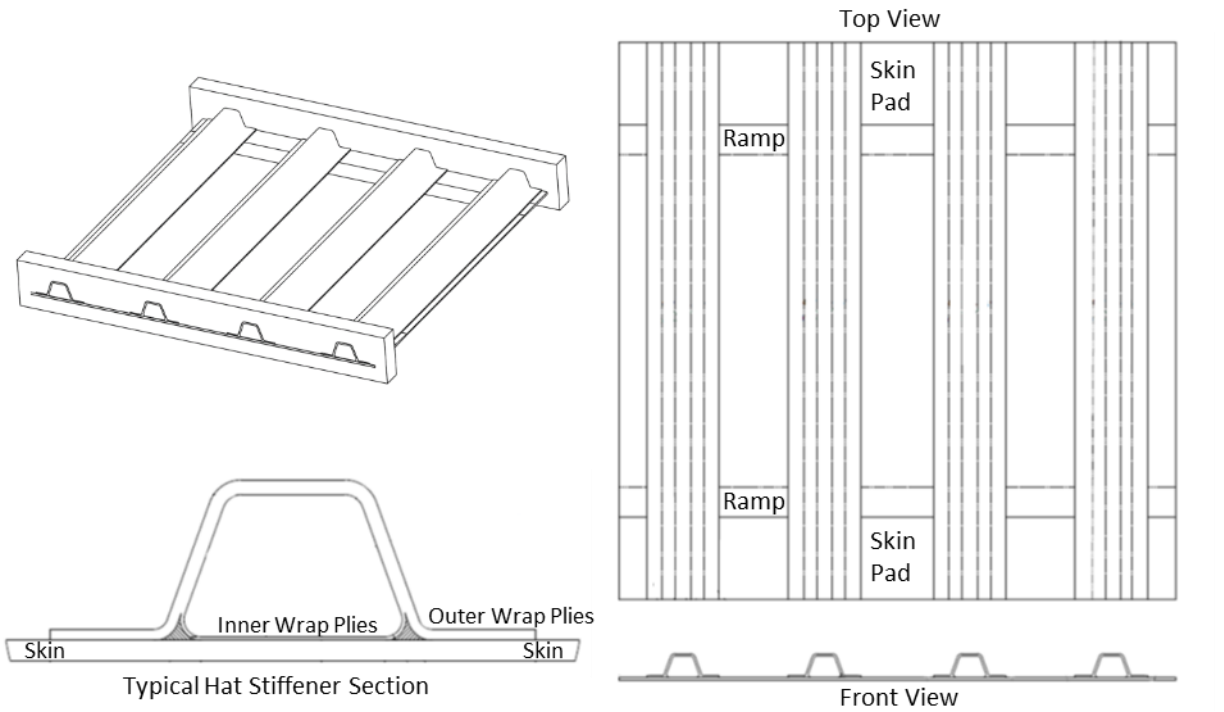

Figure 1: Multi-stringer hat-stiffened panel

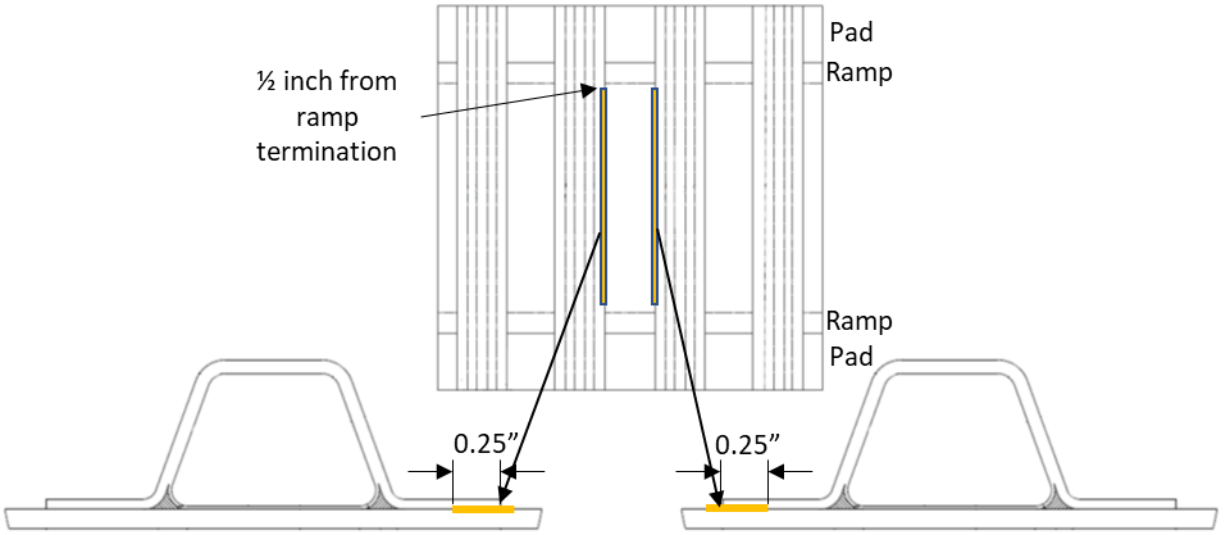

Figure 2: Location of Teflon strip in the hat stiffener-to-skin interface

III. Test results for correlation

Panel test results showed that a stable damage progression occurred in the panel prior to catastrophic failure. Reference 3 shows specific details of the test results to which the CompDam analysis results are herein compared. Each panel had back-to-back strain gages at multiple locations. Figure 3 shows the approximate strain gage locations and the global behavior of the tested panels. The panel's stiffness was calculated using the average strains recorded at each location between 20 and 40 kip applied load. A panel stiffness of approximately 4×10^6 psi was calculated at each strain gage location. The critical buckling loads were calculated from the recorded strain gage data and the digital image correlation captured during the test. All panels showed the center skin bay buckled first at an average

compressive load of 44.6 kip, followed by the two full outer skin bays at an average compressive load of 76.5 kip. Each skin bay buckled into a five half-wave shape with the center, upper, and lower wave of the buckled shape deflecting away from the stiffeners, which caused a peel mode between the stiffener flange and the skin. Passive thermography, acoustic emission, and ultrasonic inspection showed that damage occurred at each of the peel zones of the center skin bay, with no damage in the outer skin bays. The damage from the center buckle was the critical location which lead to the ultimate failure of the panel.

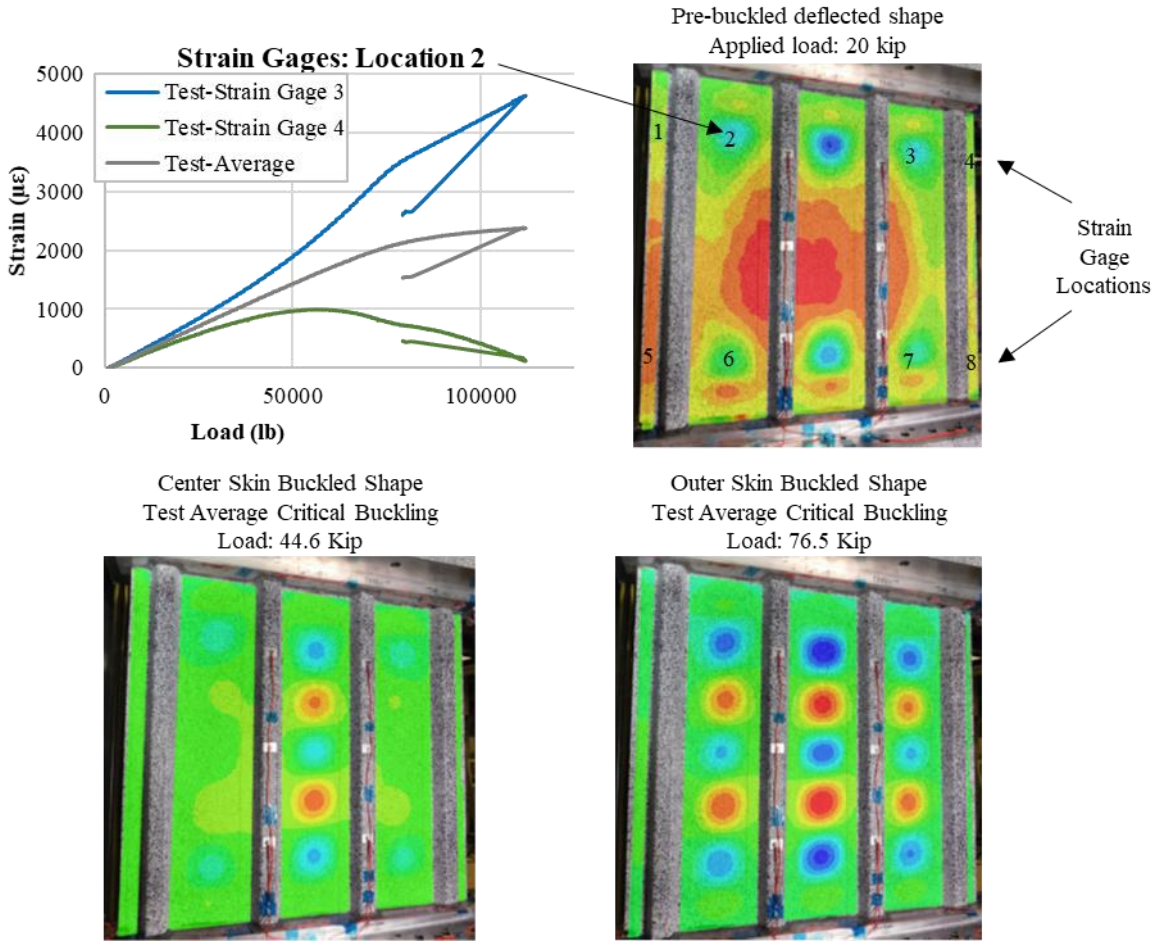

Figure 3: Buckled mode shapes of the multi-stringer panel

Figure 4 shows the incremental damage captured by ultrasonic inspection. Damage in the critical location was found to occur on both sides of the center skin bay with the same general shape. The details of the growth in the third stiffener's interface revealed that initiation occurred at approximately 106 kip applied load. The growth from the Teflon insert took on a rounded shape, which matched the local mode shape of the buckled skin. Delamination growth was found to occur in the skin-stiffener interface as well as the skin's ply1-ply2 interface. Evidence of a matrix split in ply 1 was also observed at the boundary of the skin-stiffener interface and the skin ply1-ply2 interface, leading to the conclusion that the initial growth had led to a migration of the crack from the Teflon insert in the skin-stiffener interface. As the compressive load was increased, the delamination growth continued with the same shape and migration characteristics, with most of the delamination in the skin's ply1-ply2 interface. The ultrasonic inspections in Figure 4 show the onset of a second migration to the skin's ply2-ply3 interface near peak load. This was not observed in the other incrementally loaded multi-stringer test. At peak load, the center delamination became unstable and propagated rapidly across the panel. The Teflon insert multi-stringer panels had an average peak load of 114.3 kip.

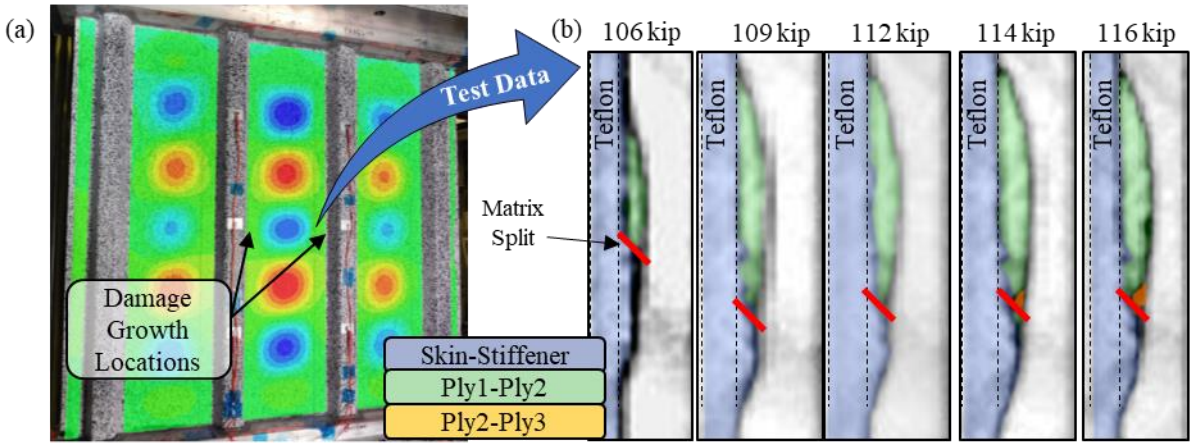

Figure 4: (a) Out of plane deflections of test panel with (b) damage propagation detected during incremental ultrasonic inspection

IV. Modeling approach

A PDFA finite element model was developed for the post-buckled multi-stringer panel with a Teflon insert. An integrated global-local approach was used to capture the overall panel behavior and the intricate local damage characteristics. The global model captured the panel's pre-buckled response, buckled mode shapes, and the post-buckled response while the CompDam PDFA method captured any delamination growth, ply cracking, and delamination migration that occurred in the local analysis region. The approach employed herein for the CompDam PDFA method was exercised and validated using smaller specimens in the ACP V&V framework, e.g., [4]. The integrated global-local approach allowed for load redistribution to occur through the entirety of the panel as the local damage progressed during the analysis.

The skin of the global model was meshed with a relatively coarse mesh, seen in Figure 5. An element size of 0.1 inches by 0.1 inches was used for the entire global region with one element through the skin thickness. The elements of the skin were continuum shell elements (SC8R) with a layered material property that was representative of the plies at each element's location.

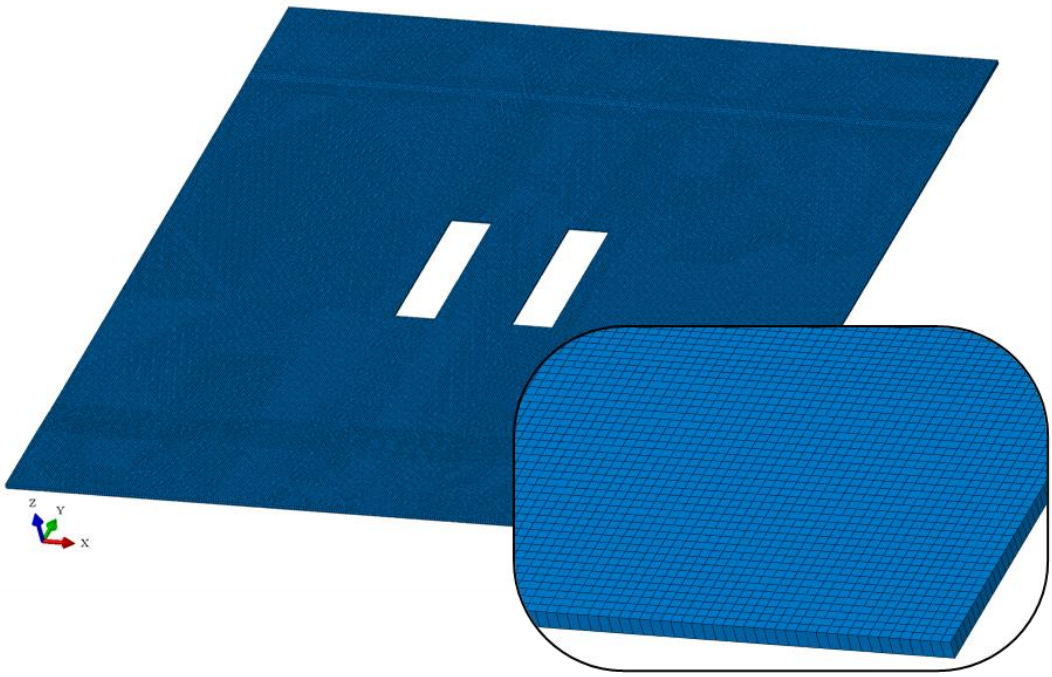

Figure 5: Global skin mesh

The full three-dimensional mesh also captured an as-manufactured feature found in the skin. The design of the end of the panel included a pad-up area where the thickness of the skin doubled. The pad-up was designed to be symmetric about the mid-plane of the skin with the upper ramp and lower ramp region aligned. When inspecting the test panels after they were manufactured, it was discovered that the upper ramp and lower ramp did not align, which produced a divot in the smooth side of the skin. This profile was applied to the global model by manually adjusting the nodes of the lower surface of the skin (non-stiffener side) to match the coordinate measuring machine data of the manufactured panels. Figure 6 shows the skin's as-manufactured mesh (blue) and the as-designed geometry (grey).

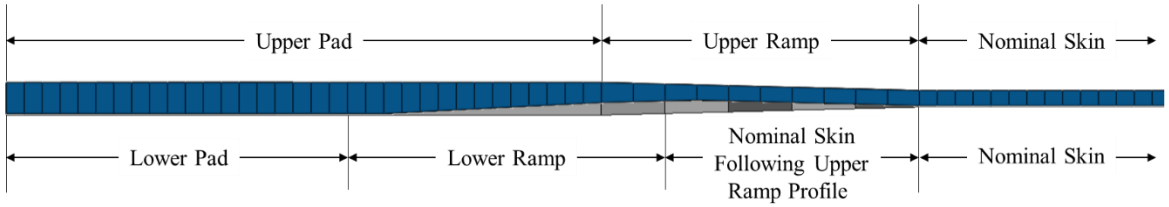

Figure 6: Side view of the pad-up end of the skin mesh

All four stiffeners were also modeled with full three-dimensional representation, as seen in Figure 7. A mesh size of 0.1 inches x 0.1 inches was selected to provide a mesh that was similar to the skin. This produced a generally regular continuum shell mesh with one element through the thickness. The area of the noodle region, where the outer wrap plies join with the inner wrap plies, was not modeled in detail, which produced an irregular reduced integration continuum solid mesh (C3D8R) in this area. The full length of the 1st and 4th stiffeners were modeled while the middle section of the 2nd and 3rd stiffeners were omitted in the global model. The lower surface of the 2nd and 3rd stiffeners also had cohesive elements (COH3D8) modeled with the same global element dimensions. The continuum shell elements of the stiffeners were given a layered material property based on the layup at the element's location. The continuum solid elements of the noodle region were given a smeared orthotropic material property that accounted for the combined stiffness of the fabric outer and inner wrap plies as well as the resin rich noodle region. The Teflon insert that was located along the full length of the stiffener flanges adjacent to the center skin bay was captured using reduced strength and fracture toughness properties to allow for these elements to fail at the beginning of the analysis. The rest of the cohesive elements were assigned stiffness, strength, and fracture toughness properties based on a crack growing in a tape-fabric interface.

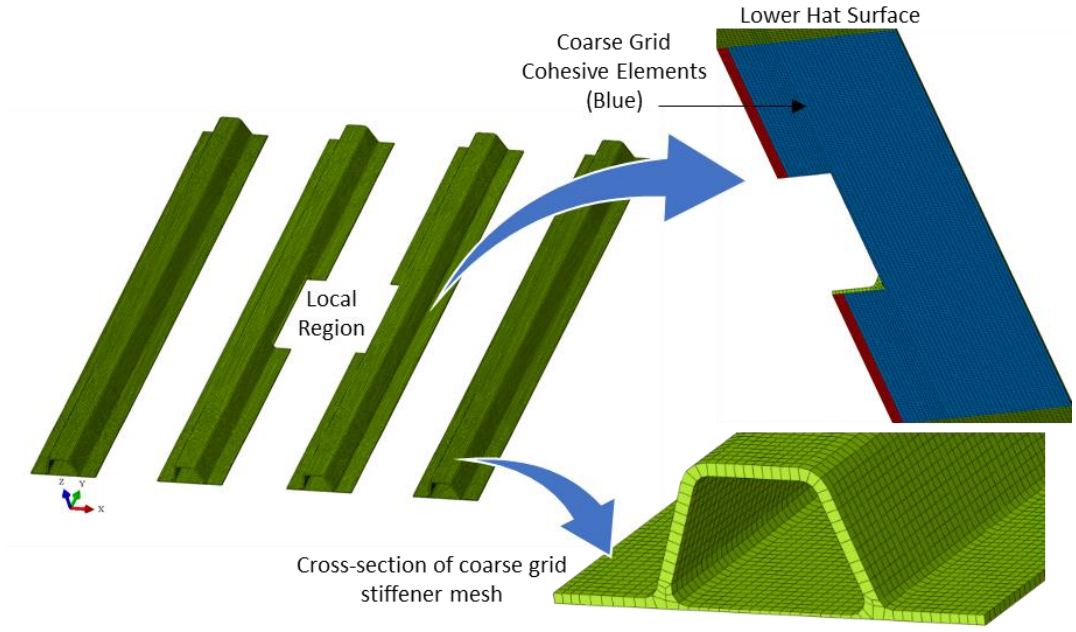

Figure 7: Global model stiffener mesh

The stiffeners and the skin of the global model were assembled using mesh ties at the intersecting surfaces. The first and fourth stiffeners of the global model were directly tied in the model, therefore no damage would occur in these areas. The second and third stiffeners of the global model had the skin tied to the lower surface of the cohesive elements. The cohesive elements allowed delamination damage to propagate during the analysis if needed.

Two local areas were incorporated into the global model. The local areas were 6 inches by 1.75 inches in size and extended through the full thickness of the assembled panel, including the hat stiffener and two discretely modeled skin plies, as seen in Figure 8. All parts of the local region were separated by cohesive elements to capture the interlaminar damage that could occur. The local regions were located at the center of the 2nd and 3rd stiffeners, adjacent to the center of the panel to capture the critical damage growth. Mesh ties were used to connect the individual layers of the local region to each other as well as the perimeter to the local region to the global model. In each of the ties, the surfaces involved were generated using the element faces instead of the nodes on the face. This resulted in a better mesh tie definition during the analysis. The mesh ties connecting the individual layers through the thickness of the local region were also configured so the surfaces of the cohesive elements were the slave surfaces of the tie definition. Separate mesh ties were used for the stiffener and skin to join the local region to the global region. The cohesive elements were not included in the global-to-local mesh ties.

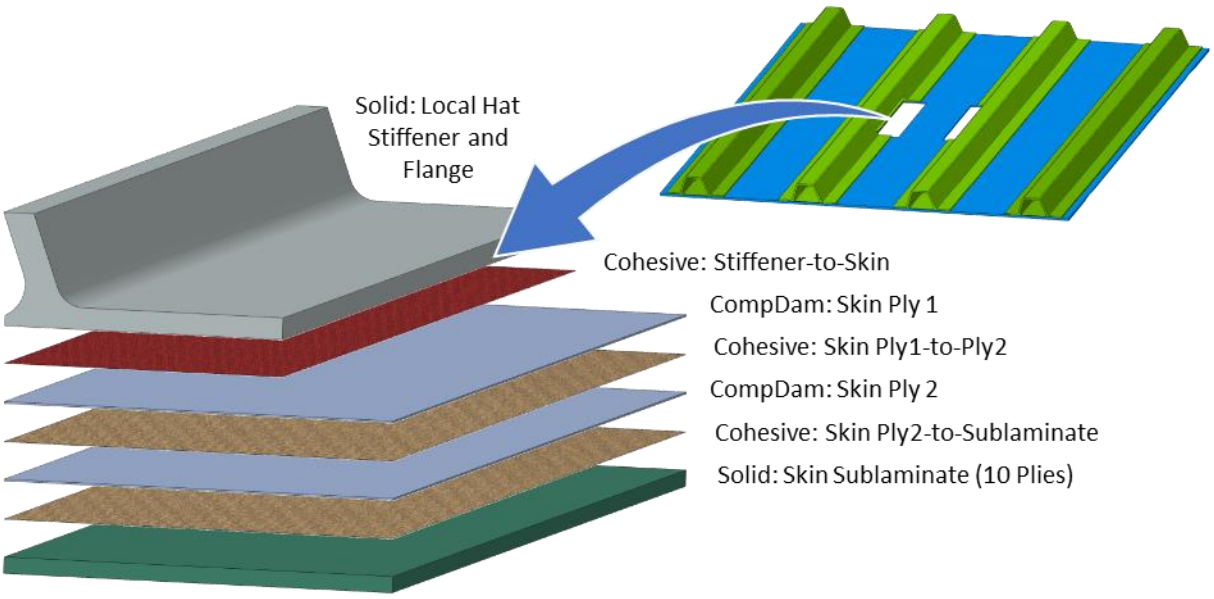

Figure 8: CompDam local model, exploded view

All parts of the local region were modeled with a planar element size of 0.01 inches by 0.01 inches. Figure 9 shows the resulting mesh for all parts of the local region. The first and second tape ply of the skin were discretely modeled with fiber-aligned, reduced integration continuum solid elements. Most of these elements were given CompDam VUMAT material properties to capture the intralaminar damage modes of the model. The remaining 10 plies of the skin were modeled with a single layer of continuum shell elements. These elements were assigned a layered material property to capture the remaining layup; no intralaminar or interlaminar damage would occur in these plies. The local region of the stiffener had enough fidelity to capture the effects of the outer wrap plies, inner wrap plies and noodle region discretely. The inner and outer wrap plies were modeled with continuum shell elements with layered material properties. The noodle region was modeled with reduced integration continuum solid elements. Intralaminar or interlaminar damage was not captured in the discretely modeled stiffener elements. The cohesive elements separating the stiffener and the first ply of the skin were given stiffness, strength and fracture toughness properties that were consistent with a crack growing in a tape-fabric interface. The cohesive elements separating the skin plies were given properties consistent with a crack growing in a tape-tape interface.

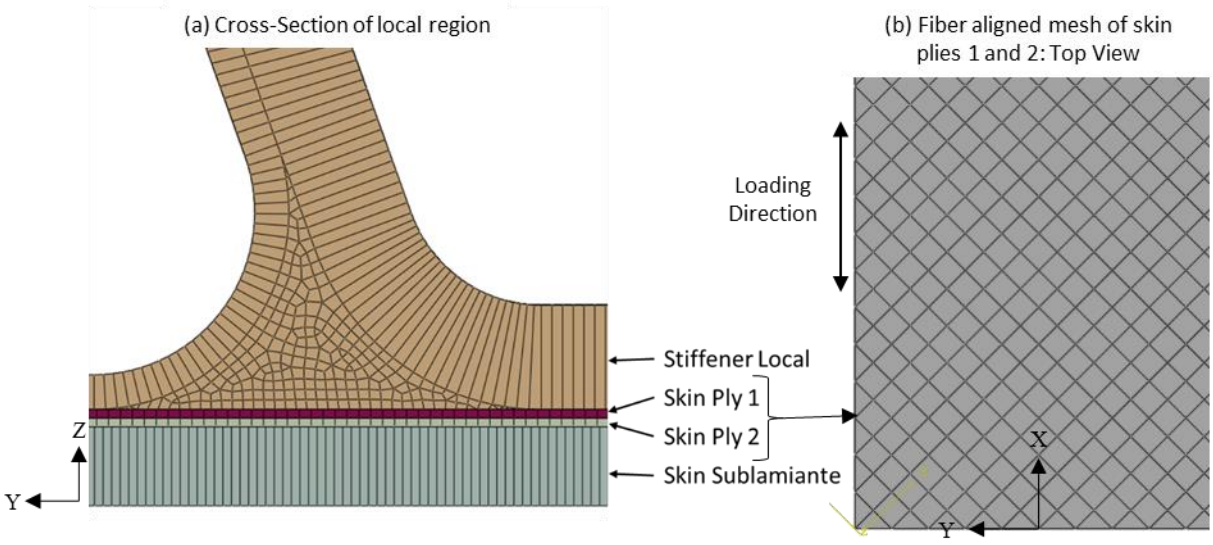

Figure 9: Local region mesh details of (a) all assembled parts and (b) the discretely modeled plies

The discretely modeled, fiber-aligned skin plies were assigned multiple material properties, as shown in Figure 10, to accurately capture the intralaminar damage modes that could occur. A local coordinate system defined the fiber direction of the elements. The perimeter elements (grey) were assigned non-damaging, linear elastic material properties to isolate the damaging elements from the mesh tie definition at the boundary of the local zone. All interior elements were assigned CompDam material properties with a different set of failure modes activated. Strips of elements following the fiber direction (orange) could fail by either (1) intralaminar cracking (matrix splits) with friction on the matrix crack surfaces or (2) fiber tensile damage. These strips of intralaminar cracking elements were separated by at least 3 strips of elements (blue) where only fiber tensile failure was considered. The strips of damaging elements continued across the entire local region to the non-damaging perimeter elements [6].

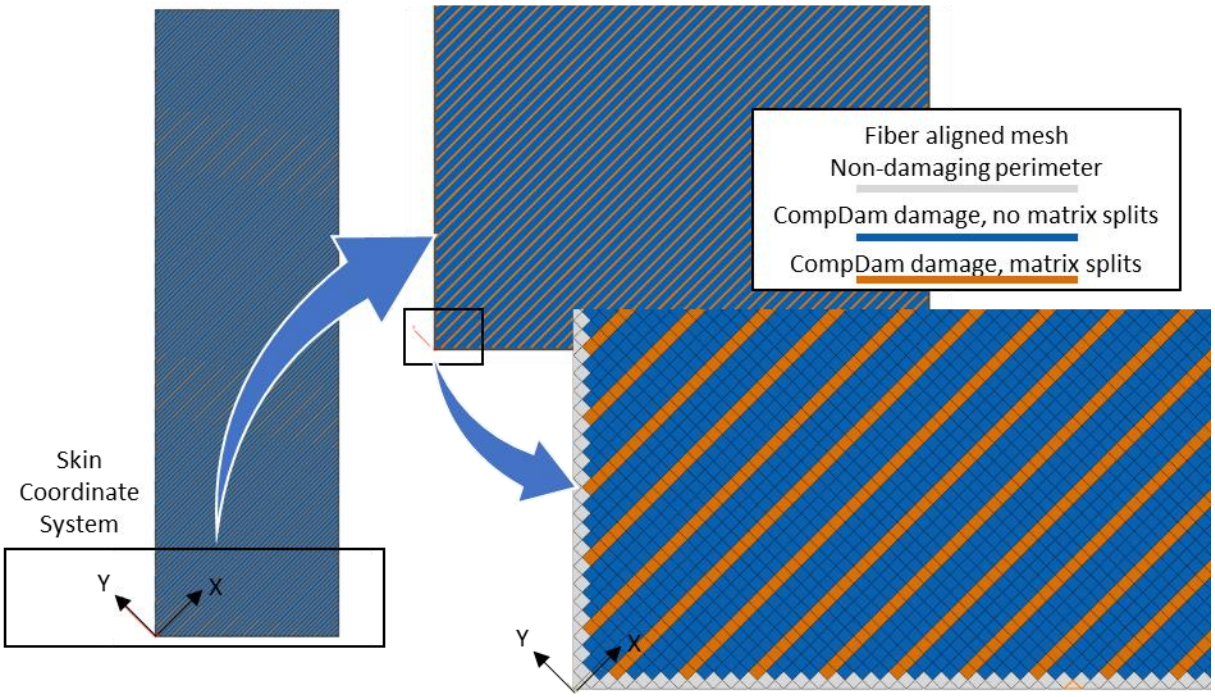

Figure 10: Fiber-aligned mesh of a 45° ply in the skin panel.

The assembled model captured the intralaminar effects of the Teflon insert along the full length of the second and third stiffener flanges adjacent to the center skin bay, as seen in Figure 11. A cohesive material property was assigned to the remaining cohesive elements between the skin and stiffener that was representative of a crack growing in a tape-fabric interface. Two sets of properties were investigated for these skin-stiffener cohesive elements. In both cases, the cohesive element's stiffness and strength properties were constant. The first set of fracture toughness values captured the critical fracture toughness (G_C) determined during typical material characterization testing. The second set of fracture toughness values represented the point at which a resistance to crack growth had fully developed (G_R) [2, 4, 6]. This phenomenon is experienced at longer crack lengths and can result in a value of G_R that is significantly higher than the critical fracture toughness values. The sensitivity of the combined intralaminar and interlaminar solution to the G_C and G_R bounds of the stiffener-skin interface was thought to provide an upper and lower bound to the tested condition.

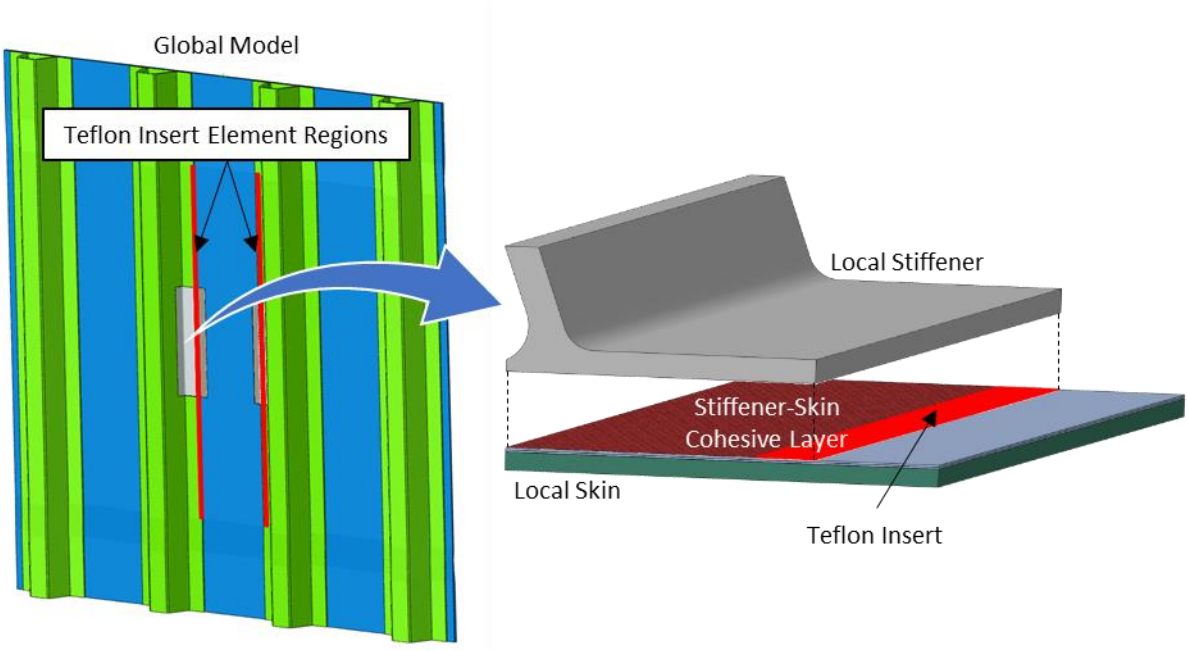

Figure 11: Teflon Insert locations on the multi-stringer panel model

The assembled global-local model contained approximately 15 million degrees of freedom. Figure 12 shows the boundary conditions applied to complete the quasi-static CompDam analysis, which was completed using the explicit solver in Abaqus 2018 and CompDam version 2.4.0. The upper edge of the model was given a compressive velocity boundary condition of 0.4 inches per second. The prescribed velocity boundary condition followed a smooth step amplitude definition to reduce the dynamic effects of the model at the beginning of the analysis. The full velocity of the loaded end of the specimen was reached at an analysis time of 0.01 seconds. The lower edge of the model was axially constrained to react the applied displacement to replicate the testing condition. The test panels had a potting material added to the upper and lower ends which was modeled as an out-of-plane restraint on those surfaces. Finally, the center point of the lower surface of the model was restrained in the transverse direction to eliminate rigid body motion of the panel. Variable mass scaling was applied during the full 0.35 second analysis time by setting a target stable time increment of 1×10^{-6} for all elements. The explicit analysis required 160 hours to complete with 96 processors and 50 GB of RAM.

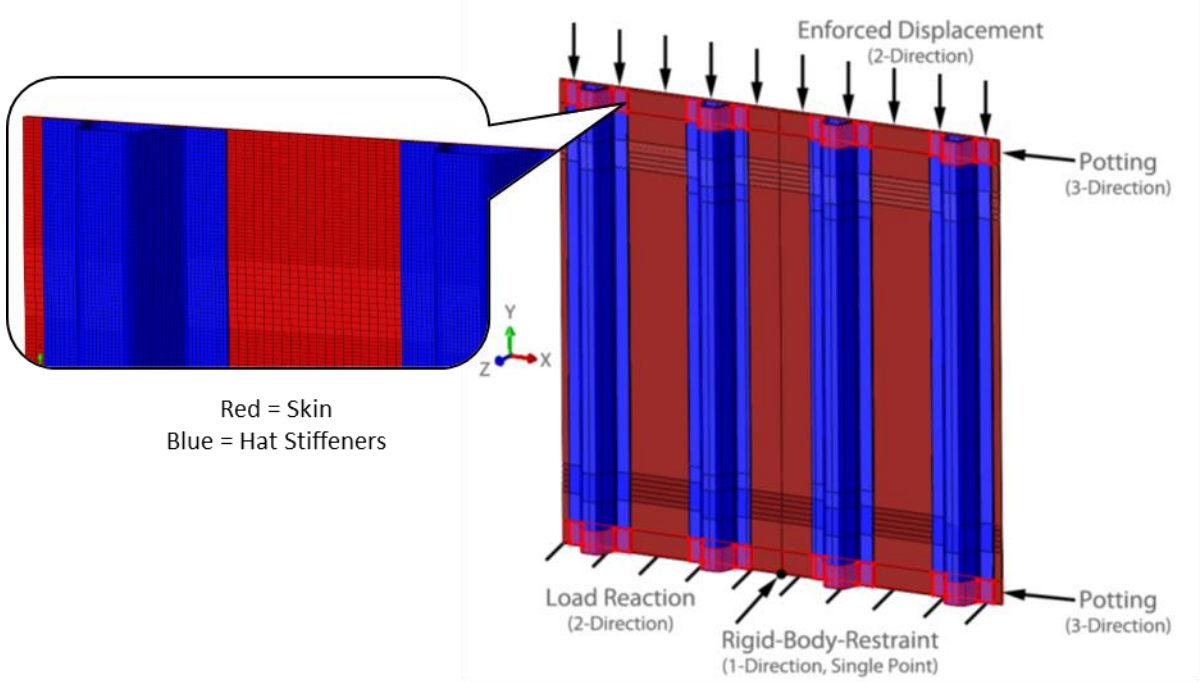

Figure 12: Coarse grid finite element model of the multi-stringer panel

V. Analysis Validation

The results of the global-to-local CompDam analysis showed excellent correlation to the test data. The global model provided an accurate representation of the pre-buckled behavior, buckling initiation loads, and buckled mode shapes while the local model accurately captured the load at which the critical damage began to grow from the Teflon insert, the overall damage patterns for both interlaminar and intralaminar damage mechanisms, and the peak load of the panel.

The pre-buckled stiffness of the panel was evaluated at each of the 8 strain gage locations on the test panel. Figure 13 shows the details of the strains captured at location 2 as well as the pre-buckled stiffness comparison. The plot shows the results of the back-to-back strains and the average strain at this location and the overall comparison to the test data. A favorable comparison between the analysis and test data was achieved. To determine the stiffness of the panel at this location, the slope of the stress/strain relationship was calculated between a load of 20,000 pounds and 40,000 pounds. This load range ensured a generally linear average pre-buckled behavior free of the initial non-linear effects in the test data. The engineering stress was calculated using the total cross-sectional area of the panel (8.934 in^2). For location 2, an error of 5.7% was calculated for the pre-buckled stiffness. Table 1 shows the comparison of the pre-buckled stiffness for the other seven strain gage locations. The maximum error of -12.5% occurred at position 1 (upper left free edge) and the minimum error of +5.7% occurred at location 2. Most of the locations had a pre-buckled stiffness error of less than 10% when compared to test data.

Table 2 shows the comparison of the critical buckling loads of the center and outer skin bays. The analysis was able to accurately capture the onset of buckling, though in both cases, it under predicted the average test values. The center skin bay showed a critical buckling load of 43.6 kip which was 2.2% less than the test average value while the outer skin bays showed a critical buckling load of 70 kip, which was 8.4% less than the test average value.

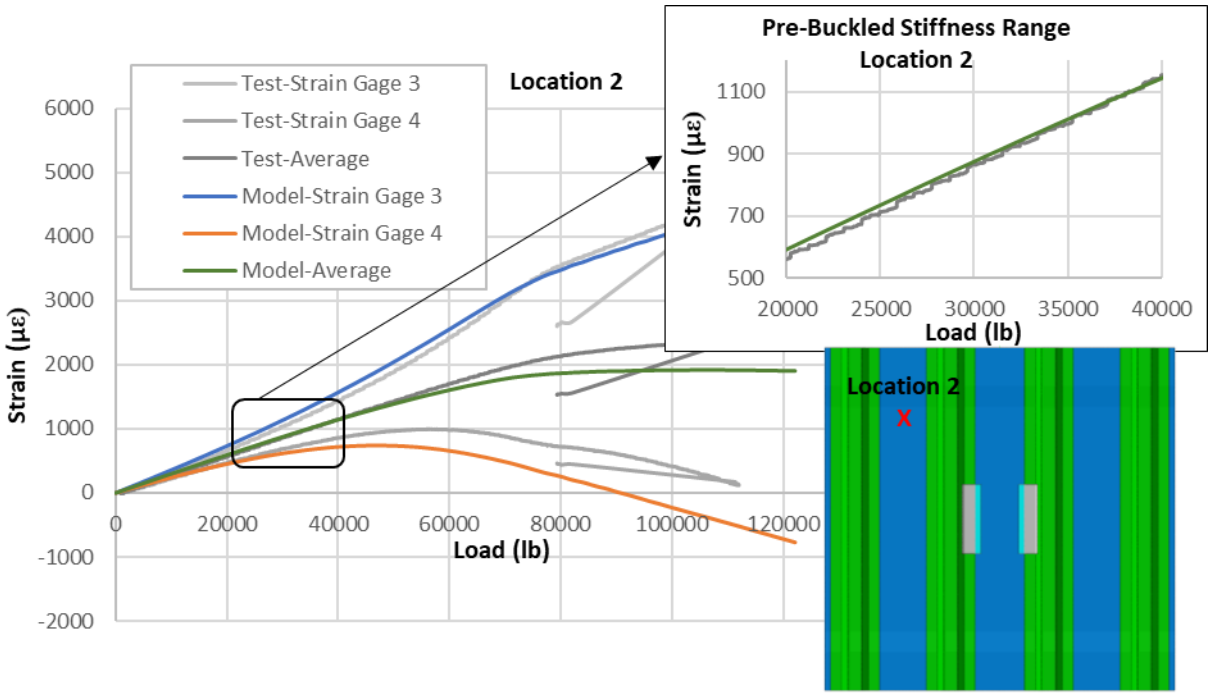

Figure 13: Pre-buckled stiffness evaluation

Table 1: Pre-buckled stiffness evaluation

Location	Test Average Stiffness ($x10^6$ psi)	Analysis Stiffness ($x10^6$ psi)	%Error
1	4.35	3.81	-12.5%
2	3.84	4.06	5.7%
3	3.88	4.11	5.8%
4	4.,32	3.79	-12.2%
5	4.22	3.88	-8.0%
6	3.62	3.99	10.2%
7	3.65	3.99	9.3%
8	4.27	3.90	-8.8%

Table 2: Critical buckling load

	Test Average Critical Buckling Load	Analysis Critical Buckling Load	%Error
Center Skin Bay	44.6 kip	43.6 kip	-2.2%
Outer Skin Bays	76.5 kip	70 kip	-8.4%

Figure 14 shows the comparison of the buckled mode shape of the center and outer skin bays for applied loads above the onset of buckling to validate the analysis results. At 55 kip applied load, the center skin bay had developed a five half-wave buckled mode shape where the center, upper, and lower half waves were deflecting away from the stiffeners (blue colored contours). The second and fourth half waves were deflecting into the stiffener (red colored

contours). This matched the test data at a similar load level. At 55 kip applied load, it can also be seen, in both the analysis and the test data, that the center skin bay had buckled while the outer skin bays had not yet buckled. At an applied load of 80 kip, the five half-wave post-buckled shape in the center skin bay had continued, and the outer skin bays had buckled into the same shape.

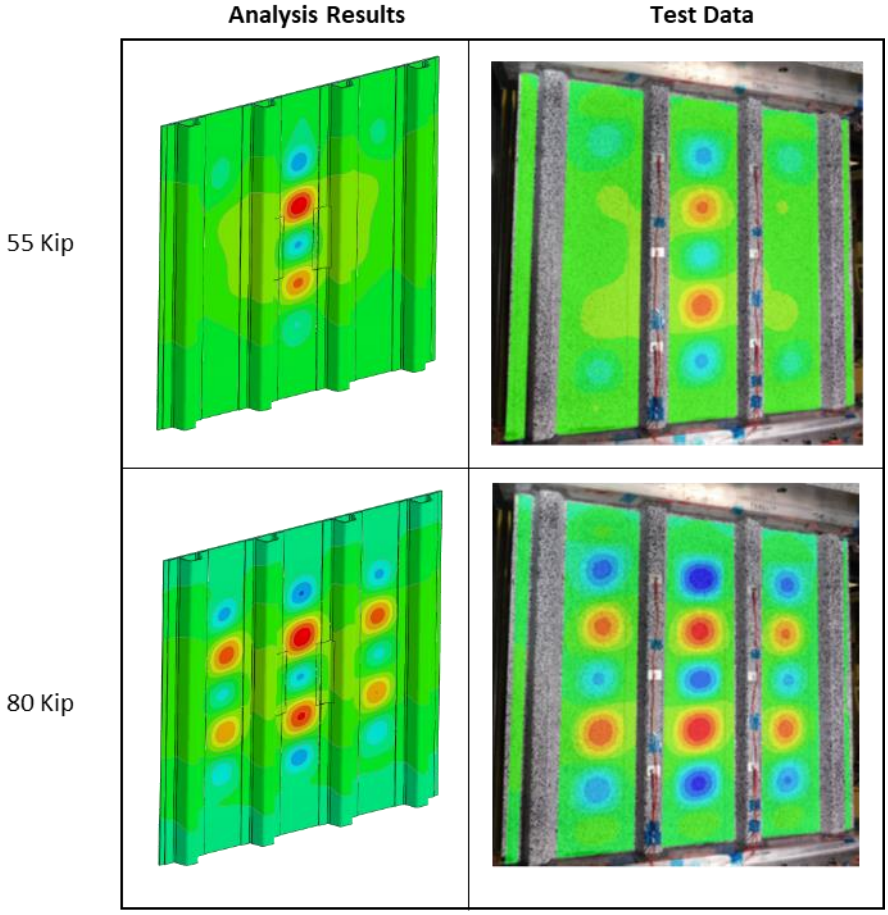

Figure 14: Buckled Mode Shape Comparison

The buckled mode shapes remained as additional load was applied to the panel. The progressive damage analysis of the model was focused on skin-stiffener flanges adjacent to the central half-wave of the center skin bay as this was determined to be the critical location for panel failure. Damage initiation was determined to occur when either a matrix split in ply 1 had fully developed or a cohesive element in the area had fully degraded. The load at which either of these events happened was then compared to the average first indication of damage seen in the test data. In the multi-stringer panel analysis where the tape-fabric interfacial properties used the initiation (G_C) fracture toughness values, the onset of damage was determined to occur at 112.7 kip applied load. This was 4.9% higher than the test average value of 107.5 kip.

Figure 15 shows the comparison of the damage evolution between the tested panels and the CompDam analysis. At 112.7 kip, the CompDam analysis had initiated delamination damage in the skin-stiffener interface at the middle of the panel. As additional displacement was applied, the delamination in the skin-stiffener interface grew along the length of the Teflon edge. At a load of 117.9 kip, the analysis showed that the overall rounded shape of the delaminated area had continued to grow in both length and depth into the stiffener; however, multiple matrix splits had occurred in ply1 of the skin along the Teflon edge. These matrix splits allowed the delamination growing in the skin-stiffener interface to migrate to the skin ply1-ply2 interface. As the load increased, many of the matrix splits in ply 1 had experienced some growth, mostly under the Teflon insert towards the center of the panel. One of the matrix splits in ply 1 experienced significant growth towards the stiffener and was the critical matrix split which allowed the delamination migration from the skin-stiffener interface to the skin ply1-ply2 interface to occur. At the maximum load

of the analysis, the amount of delaminated area between the two affected interfaces was approximately equal. This generally agreed with the test data. In testing, a significant amount of delaminated area appeared at 106 kip. This damaged area showed a generally rounded shape and an even distribution of damage in the skin-stiffener interface and the skin ply1-ply2 interface. There was also evidence of a matrix split in ply 1, allowing the migration of the delamination. As additional displacement was applied, the delaminated area grew mostly along the length of the stiffener with a little bit of growth into the stiffener. Most of the delamination growth occurred in the skin ply1-ply2 interface with evidence of multiple matrix splits in ply 1 of the skin along the Teflon edge. Near the peak load of the test, a second migration was found to the skin ply1-ply2 interface, though this was not seen in all incremental testing.

The maximum load achieved by the analysis was 120.2 kip, which was 5.1% higher than the average testing peak load of 114.4 kip. This peak analytical load was preceded by rapidly increasing rate of crack growth, as shown in Figure 15.

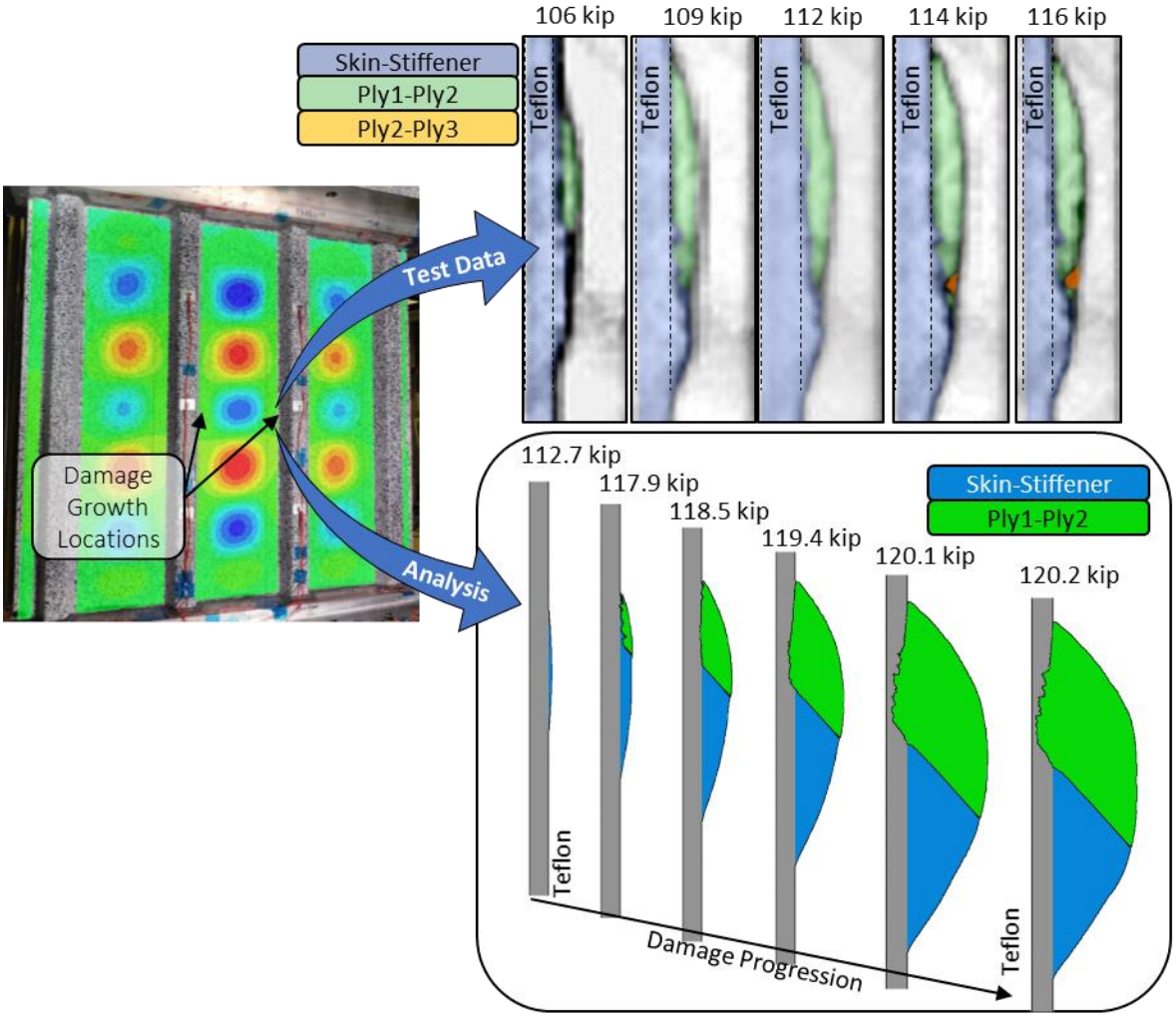

Figure 15: Progressive damage results for the multi-stringer panel with G_C interfacial fracture toughness

It was expected that the higher fracture toughness values (G_R) of a fully developed resistance curve for the tape-fabric interface would provide an upper bound analysis to the test panel behavior. The stiffness and buckling validation evaluation criteria were unchanged from the G_C analysis results. Figure 16 shows the resulting progressive damage solution achieved in the local region of the model with the G_R interfacial properties. The damage initiation load was increased to 123.8 kip, which was 15.2% higher than the test average value. The damage initiation mode was also changed by the interfacial property update. With the tougher tape-fabric interface, the initial damage in the local region was matrix splits through the thickness of ply 1 instead of delamination damage to the skin-stiffener interface. As load was increased, delamination occurred first in the skin ply1-ply2 interface along with the additional growth of matrix

splits in ply 1. At a load of 125.4 kip, a matrix split had opened significantly enough to allow the growing delamination to migrate to the skin-stiffener interface at the lower end of the delamination front. As load was increased up to the peak load, the rounded delaminated continued to grow along the length of the stiffener and into the stiffener. Most of the delaminated area occurred in the skin ply1-ply2 interface with one significant matrix split allowing the migration to the skin-stiffener interface. The distribution of delamination growth between the skin-stiffener interface and the skin ply1-ply2 interface produced by the analysis using G_R agreed better with the test data than the results using G_c did. The peak load of 128.3 kip was 12.2% higher than the average test data.

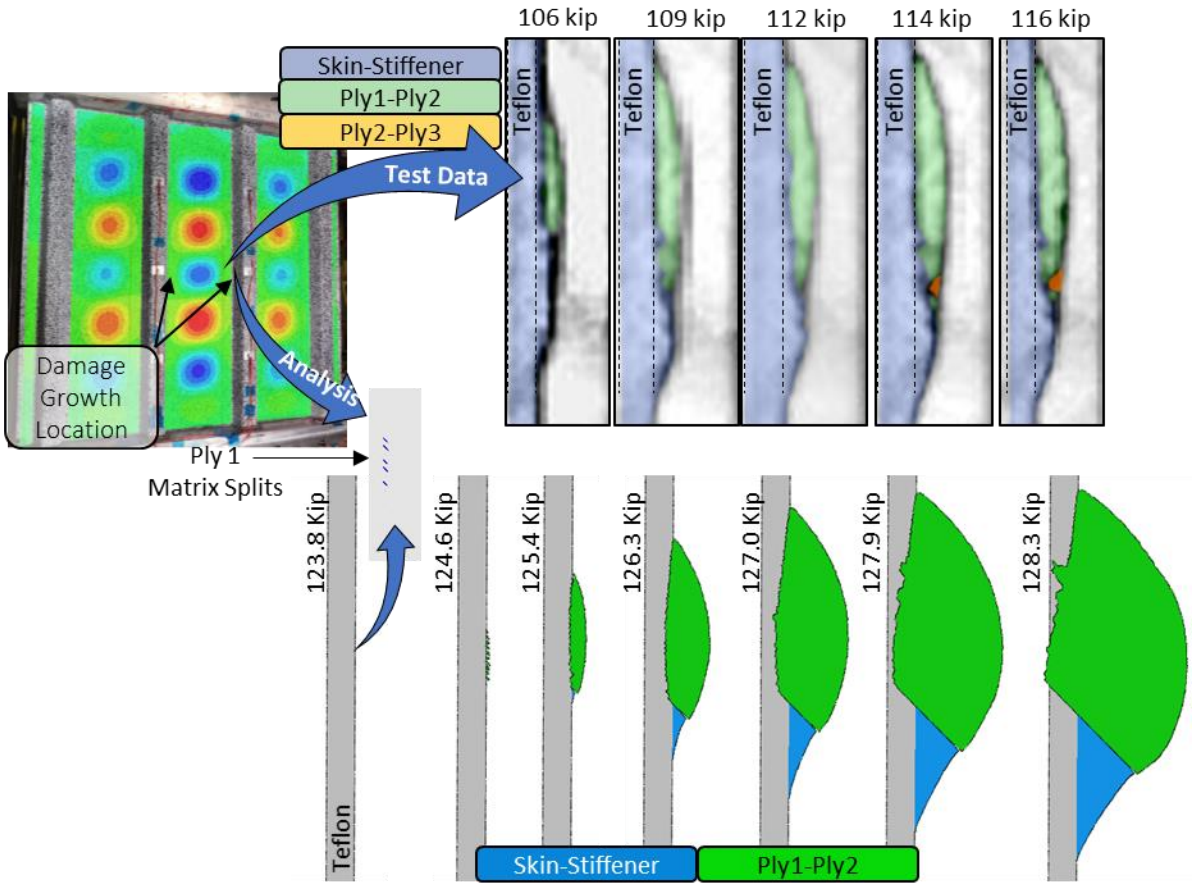

Figure 16: Progressive damage results for the multi-stringer panel with G_R interfacial fracture toughness

VI. Conclusion

The validation of a large multi-stringer panel model with a Teflon insert was completed using CompDam PDFA methodology to capture a complex interaction of interlaminar and intralaminar failure modes. The global-to-local modeling approach adequately captured the pre-buckled behavior of the panel, the critical buckling load of the center and outer skin bays, the buckled mode shape, the load at which damage initiates, the characteristics of the overall damage morphology, and the peak load of the panel. The stiffness validation of the analysis showed an error range from 12.5% under-predicted to 10.2% over-predicted for the 8 locations. Most of the locations had a stiffness that was within 10% of the test average value. In general, the model accurately captured an average stiffness of 4 x10^6 psi. The onset of buckling of the center skin bay was calculated to be within 3% of the test average value and the outer skin bays within 9%. The analysis accurately captured the five half-wave buckled mode shape seen in the testing.

With a tape-fabric critical interfacial fracture toughness property (G_C) applied to the skin-stiffener cohesive elements, the onset of damage growth was calculated to occur at the center of the panel within 5% of the tested panels. The damage morphology of the analysis generally developed into a larger area than what was seen in testing and took on a more rounded shape. The analysis accurately predicted the presence of a single critical matrix split that would allow a migration between the skin-stiffener interface and skin's ply1-ply2 interface, with other non-critical matrix splits being present. The distribution of crack growth between the two interfaces was about even in the analysis, which

was not the case found in the test data. The peak load of 120.2 kip was approximately 5% above the average peak load of the test.

When the skin-stiffener interfacial properties were updated to the higher, fully developed resistance curve fracture toughness values (G_R), a different local behavior was achieved. The G_R analysis showed an increase in the onset of damage load to 123.8 kip, which was 15% higher than the test average. The failure mode at the onset of damage growth was changed from a delamination in the skin-stiffener interface to a matrix split in ply 1. From the initial matrix split, the initial delamination growth occurred in the skin's ply1-ply2 interface with multiple matrix splits in ply 1 until a single critical matrix split was encountered which allowed the delamination to migrate to the skin-stiffener interface. Continued delamination growth up to the peak load of 128.3 kip had a generally rounded damage morphology with most of the delamination being contained in the skin's ply1-ply2 interface. The peak load of the G_R analysis was 12% higher than the average peak load of the testing.

References

1. Rose, C. A., Davila, C. G., and Leone, F. A., "Analysis Methods for Progressive Damage of Composite Structures. NASA/TM-2013-218024," 2013.
2. Leone, F.A., Song, K., Johnston, W., Rose, C.A., Jackson, W.C., Kosztowny C.J., Davila, C.G., "Test/Analysis Correlation of Damage States in Post-buckled Stiffened Validation Building Block Specimens," American Society for Composites 34th Technical Conference, 2019.
3. Action, J., Jackson, W., Zalameda, J., Palliyaguru, U., "Testing of a Multi-Stringer Post-Buckled Panel," AIAA Scitech 2020 Technical Conference, Orlando, FL, 2020.
4. Selvarathinam, A., De Carvalho, N. V., Seshadri, B.R., Johnson, V. E., Johnston, W., "Validation of Floating Node Method Using Three-Point Bend Doubler Under Quasi-Static Loading," AIAA SciTech 2019 Technical Conference, San Diego, CA.
5. Hyder, I., Leone, F. A., Justusson, B., Schaefer, J., Bergan, A., Wanthal, S., "Implementation of a Matrix Crack Spacing Parameter in a Continuum Damage Mechanics Finite Element Model," American Society for Composites 33rd Technical Conference, 2018.
6. Foote, R. M. L., Mai, Y.-W., and Cotterell, B., "Crack Growth Resistance Curves in Strain Softening Materials," *Journal of the Mechanics and Physics of Solids*, Vol. 34, No. 6, pp. 593- 607, 1986.